# Topological Phase for Spin-Orbit Transformations on a Laser Beam

C. E. R. Souza,[1] J. A. O. Huguenin,[1] P. Milman,[2] and A. Z. Khoury[1]

[1]*Instituto de Física, Universidade Federal Fluminense, 24210-340 Niterói-RJ, Brasil*

[2]*Laboratoire Matériaux et Phenomènes quantiques CNRS UMR 7162, Université Denis Diderot, 2 Place Jussieu, 75005 Paris cedex, France*

(Received 29 March 2007; published 15 October 2007)

We investigate the topological phase associated with the double connectedness of the $SO(3)$ representation in terms of maximally entangled states. An experimental demonstration is provided in the context of polarization and spatial mode transformations of a laser beam carrying orbital angular momentum. The topological phase is evidenced through interferometric measurements, and a quantitative relationship between the concurrence and the fringes visibility is derived. Both the quantum and the classical regimes were investigated.

DOI: 10.1103/PhysRevLett.99.160401 PACS numbers: 03.65.Vf, 03.67.Mn, 07.60.Ly, 42.50.Dv

The seminal work by Pancharatnam [1] introduced the notion of the geometric phase associated with cyclic polarization transformations. A quantum mechanical parallel for this phase was later provided by Berry [2]. Recently, the interest for geometric phases was renewed by their potential applications to quantum computation. The experimental demonstration of a conditional phase gate was recently provided in both nuclear magnetic resonance [3] and trapped ions [4]. Another optical manifestation of geometric phase is the one acquired by cyclic spatial mode conversions of optical vortices. This kind of geometric phase was first proposed by van Enk [5] and recently found in a beautiful demonstration by Galvez *et al.* [6].

Pure states of a single qubit can be represented on the surface of the Bloch sphere for spin $1/2$ particles or the Poincaré sphere for polarization states. A Poincaré sphere representation can also be constructed for first order spatial modes of an optical beam [7]. Therefore, in the quantum domain, we can attribute two qubits to a single photon, one related to its polarization state and another one to its spatial structure. Geometrical phases of a single qubit can be interpreted in such representations as being related to the solid angle of a closed trajectory. However, in order to compute the total phase gained in a cyclic evolution, one should also consider the dynamical phase. When added to the geometrical phase, it leads to a total phase gain of $\pi$ after a cyclic trajectory. This phase has been put into evidence for the first time using neutron interference [8]. The appearance of this $\pi$ phase is due to the double connectedness of the three dimensional rotation group $SO(3)$. However, in the neutron experience, only two dimensional rotations were used, and this topological property of $SO(3)$ was not unambiguously put into evidence, as explained in details in [9,10].

As discussed by Milman and Mosseri [9,10], it is possible to put into evidence this topological property of $SO(3)$ using maximally entangled states (MES). It was shown in [11] that MES are in bi-univocal correspondence with $SO(3)$, so one can associate one MES to each point of the space of three dimensional rotations. In this way, MES are solely represented on the volume of the $SO(3)$ sphere that has radius $\pi$ and its diametrically opposite points identified. This construction reveals two kinds of cyclic evolutions, each one mapped to a different homotopy class of closed trajectories in the $SO(3)$ sphere. One kind is mapped to closed trajectories that do not cross the surface of the sphere (0-type) and the other one is mapped to trajectories that cross the surface ($\pi$-type). The phase acquired by a maximally entangled state is 0 for the first kind and $\pi$ for the second one. Notice that for MES evolving under local unitary transformations, the dynamical and geometrical phases can be calculated, and they provide null contribution to the global phase. Total phase is purely of topological origin. For *pure* non-MES, Ref. [11] also proposes a geometrical representation based on the combination of the $SO(3)$ sphere and a single qubit Bloch sphere, obtained after the second qubit is traced out. Using this representation, Ref. [10] shows that the phase acquired through a cyclic evolution has a more complex structure and can be separated in three contributions: dynamical, geometrical, and topological, which add up to a total value of $\pi$ or 0. The naive sum of independent phases, one for each qubit, is applicable only for product states, and the parallel between the cyclic phase and the topological properties of $SO(3)$ is not direct. In this case, the two qubits are geometrically represented by two independent Bloch spheres.

In the present work we demonstrate the topological phase associated with polarization and spatial mode transformations of an optical vortice. This is the first experiment unambiguously showing the double connectedness of the rotation group $SO(3)$. The optical modes used in our experiment have a mathematical structure analog to the one of entangled states, so that the geometrical representation developed in [11] also applies and the results of Refs. [9,10] can be experimentally demonstrated. We investigate the analogs of both a MES and a non-MES, and provide an interference based criterium to determine the

 

mode separability. This criterium constitutes a strong evidence of the topological nature of the phase acquired in a cyclic evolution. Finally, we briefly discuss the transition of our results to the quantum regime.

Let us now combine the spin and orbital degrees of freedom in the framework of the classical theory in order to build the same geometric representation applicable to a two-qubit quantum state. Consider a general first order spatial mode with arbitrary polarization state:

$$\mathbf{E}(\mathbf{r}) = \alpha\psi_+(\mathbf{r})\hat{\mathbf{e}}_H + \beta\psi_+(\mathbf{r})\hat{\mathbf{e}}_V + \gamma\psi_-(\mathbf{r})\hat{\mathbf{e}}_H + \delta\psi_-(\mathbf{r})\hat{\mathbf{e}}_V, \quad (1)$$

where $\hat{\mathbf{e}}_{H(V)}$ are two linear polarization unit vectors along two orthogonal directions $H$ and $V$, and $\psi_\pm(\mathbf{r})$ are the normalized first order Laguerre-Gaussian profiles that are orthogonal solutions of the paraxial wave equation [12]. We may now define two classes of spatial-polarization modes: the separable ($S$) and the nonseparable (NS) ones. The $S$ modes are of the form

$$\mathbf{E}(\mathbf{r}) = [\alpha_+\psi_+(\mathbf{r}) + \alpha_-\psi_+(\mathbf{r})](\beta_H\hat{\mathbf{e}}_H + \beta_V\hat{\mathbf{e}}_V). \quad (2)$$

For these modes, a single polarization state can be attributed to the whole wave front of the paraxial beam. They play the role of separable two-qubit quantum states.

For nonseparable (NS) paraxial modes, the polarization state varies across the wave front. As for entanglement in two-qubit quantum states, the separability of a paraxial mode can be quantified by the analogous definition of concurrence. For the spin-orbit mode described by Eq. (1), it is given by

$$C = 2\,|\,\alpha\delta - \beta\gamma\,|\,. \quad (3)$$

Let us first consider the maximally nonseparable modes (MNS) of the form

$$\mathbf{E}(\mathbf{r}) = \alpha\psi_+(\mathbf{r})\hat{\mathbf{e}}_H + \beta\psi_+(\mathbf{r})\hat{\mathbf{e}}_V - \beta^*\psi_-(\mathbf{r})\hat{\mathbf{e}}_H + \alpha^*\psi_-(\mathbf{r})\hat{\mathbf{e}}_V. \quad (4)$$

For these modes $C = 1$. It is important to mention that the concept of entanglement does not apply to the MNS mode, since the object described by Eq. (4) is not a quantum state, but a classical amplitude. However, we can build an $SO(3)$ representation of the MNS modes as it was done in Refs. [10,13]. Let us define the following normalized MNS modes:

$$\begin{aligned}
\mathbf{E}_1(\mathbf{r}) &= \frac{1}{\sqrt{2}}[\psi_+(\mathbf{r})\hat{\mathbf{e}}_H + \psi_-(\mathbf{r})\hat{\mathbf{e}}_V],\\
\mathbf{E}_2(\mathbf{r}) &= \frac{-i}{\sqrt{2}}[\psi_+(\mathbf{r})\hat{\mathbf{e}}_H - \psi_-(\mathbf{r})\hat{\mathbf{e}}_V],\\
\mathbf{E}_3(\mathbf{r}) &= \frac{-i}{\sqrt{2}}[\psi_+(\mathbf{r})\hat{\mathbf{e}}_V + \psi_-(\mathbf{r})\hat{\mathbf{e}}_H],\\
\mathbf{E}_4(\mathbf{r}) &= \frac{1}{\sqrt{2}}[\psi_+(\mathbf{r})\hat{\mathbf{e}}_V - \psi_-(\mathbf{r})\hat{\mathbf{e}}_H].
\end{aligned} \quad (5)$$

Each point in the volume of the $SO(3)$ sphere corresponds to a MNS mode and points diametrically opposite are identified, which means that they correspond to the *same* mode. In Ref. [13] the reader will find a detailed description of the parametrization in the $SO(3)$ sphere. The four modes described by Eqs. (5) are represented in the following way: mode $\mathbf{E}_1$ is represented by the center of the sphere, while modes $\mathbf{E}_2$, $\mathbf{E}_3$, and $\mathbf{E}_4$ are represented by three points on the surface, connected to the center by three mutually orthogonal segments, as described in Fig. 1.

In order to evidence the topological phase for cyclic transformations, we must follow two different closed paths, each one belonging to a different homotopy class, and compare their phases. The experimental setup is sketched in Fig. 2. First, a linearly polarized $\mathrm{TEM}_{00}$ laser mode is diffracted on a forked grating used to generate Laguerre-Gaussian beams [14]. The two side orders carrying the $\psi_+(\mathbf{r})$ and $\psi_-(\mathbf{r})$ spatial modes are transmitted through half wave plates HWP-A and HWP-B, followed by two orthogonal polarizers Pol-V and Pol-H, and finally recombined at a beam splitter (BS-1). Half wave plates HWP-A and HWP-B are oriented so that their fast axes are parallel. This allows us to adjust the mode separability at the output of BS-1 without changing the corresponding output power, which prevents normalization issues.

Experimentally, a MNS mode is produced when both HWP-A and HWP-B are oriented at 22.5°, so that the setup prepares mode $\mathbf{E}_1$ located at the center of the sphere. Other MNS modes can then be obtained by unitary transformations in only 1 degree of freedom. Since polarization is far easier to operate than spatial modes, we choose to implement the cyclic transformations in the $SO(3)$ sphere using wave plates. The MNS mode $\mathbf{E}_1$ is first transmitted through three wave plates. The first one (HWP-1) is oriented at 0° and makes the transformation $\mathbf{E}_1 \rightarrow \mathbf{E}_2$, the second one (HWP-2) is oriented at −45° and makes the transformation $\mathbf{E}_2 \rightarrow \mathbf{E}_3$, and the third one (HWP-3) is oriented at 90° and makes the transformation $\mathbf{E}_3 \rightarrow \mathbf{E}_4$. All these transformations are represented by the solid lines in the diagram of Fig. 1.

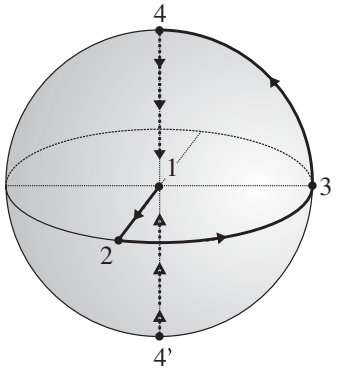


FIG. 1. Diagram representing the transformations performed in the $SO(3)$ sphere.

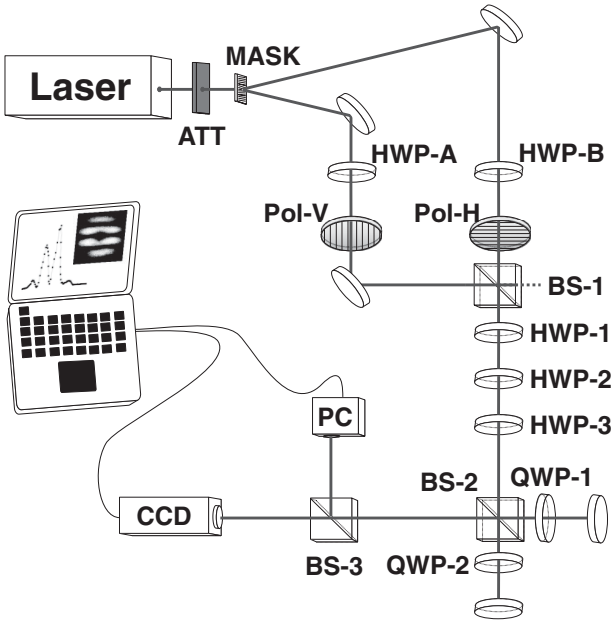


FIG. 2. Experimental setup.

Finally, two alternative closures of the path are performed in a Michelson interferometer. In one arm a $\pi$-type closure is implemented by a double passage through a quarter-wave plate (QWP-1) fixed at $-45°$. This is our fixed phase reference, and the corresponding closure is described by the dashed line connecting point $4'$ to point 1 of Fig. 1. In the other arm, either a 0-type ($4 \longrightarrow 1$) or a $\pi$-type ($4' \longrightarrow 1$) closure is performed by a double passage through another quarter-wave plate (QWP-2) oriented at a variable angle between $-45°$ ($\pi$-type) and $45°$ (0-type). These trajectories are analogous to spin rotations around different directions of space [13]. They evidence the topological properties of the three dimensional rotation group. The closed path used in the experiment is the one requiring the minimum number of wave plates and allowing the most compact interferometer, so that we could obtain stable interference fringes. We shall leave to a future work a presentation of more complicated trajectories and an extension of the phase shift to statistical mixtures.

In order to provide spatial interference fringes, the interferometer was slightly misaligned. The interference patterns were registered with either a charge coupled device (CCD) camera or a photocounter (PC), depending on the working power.

First, we registered the interference patterns obtained when an intense beam is sent through the apparatus. The images shown in Fig. 3(a) demonstrate clearly the $\pi$ topological phase shift. The phase singularity characteristic of Laguerre-Gaussian beams can easily be identified in the images and is very useful to evidence the phase shift. When both arms perform the same kind of trajectory in the $SO(3)$ sphere (QWP-1 and QWP-2 oriented at $-45°$), a bright fringe falls on the phase singularity. When QWP-2 is oriented at $45°$, the trajectory performed in each arm

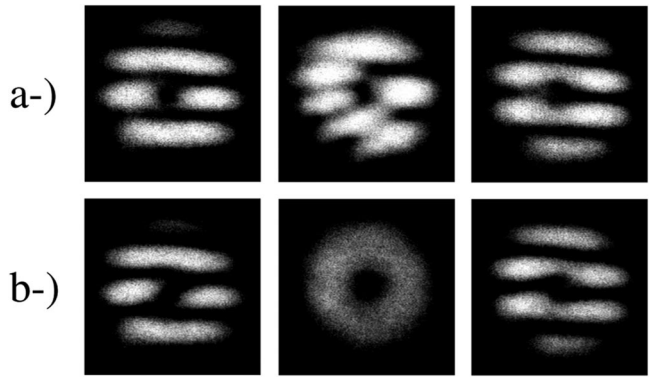


FIG. 3. Interference patterns for (a-) a maximally nonseparable, and (b-) a separable mode. From left to right the images were obtained with QWP-2 oriented at $-45°$, $0°$, and $45°$, respectively.

belongs to a different homotopy class and a dark fringe falls on the singularity, which clearly demonstrates the $\pi$ topological phase shift.

Usually, in formal derivations of geometrical and topological phases, a nice expression of the state evolution is presented where factorized phase terms appear, each one attributed to a different nature. Experimentally, we must conceive a setup in which all phase contributions vanish except the one we are interested in. The topological nature of the phase factor presented in Ref. [9] is related to the state nonseparability. Once the mode sent through the apparatus is nonseparable, a topological phase is observed. When QWP-2 is rotated from $-45°$ to $45°$, the interference fringes are deformed and finally return to their initial topology with the $\pi$ phase shift. This is clearly illustrated by the intermediate image displayed in Fig. 3(a), which corresponds to QWP-2 oriented at $0°$ [open trajectory in the $SO(3)$ sphere]. Notice that, despite the deformation, the interference fringes display high visibility. We shall see shortly that the mode separability is related to the fringes visibility.

As we mentioned above, the mode preparation settings can be adjusted in order to provide a separable mode. For example, when we set HWP-A and B both at $45°$, the output of BS-1 is the separable mode $\psi_+(\mathbf{r})\hat{\mathbf{e}}_H$. The same $\pi$ phase shift can be observed when QWP-2 is rotated, but the transition is essentially different. The interference pattern is not topologically deformed, but its visibility decreases until it completely vanishes at $0°$, and then reappears with the $\pi$ phase shift. This transition is clearly illustrated by the three patterns displayed in Fig. 3(b). In this case, the $\pi$ phase shift is of purely geometric nature, since the spatial mode is kept fixed while the polarization mode is turned around the equator of the corresponding Poincaré sphere.

The relationship between mode separability and fringes visibility can be clarified by a straightforward calculation of the interference pattern. Let us consider that HWP-A and B are oriented so that the output of BS-1 is described

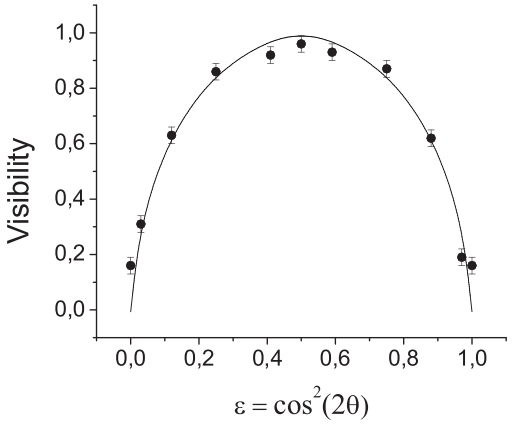


FIG. 4. Fringes visibility as a function of $\epsilon$. The solid line is a theoretical fit with $C = 2\sqrt{\epsilon(1-\epsilon)}$.

by

$$\mathbf{E}_{\epsilon}(\mathbf{r}) = \sqrt{\epsilon}\psi_{+}(\mathbf{r})\hat{\mathbf{e}}_{H} + \sqrt{1-\epsilon}\psi_{-}(\mathbf{r})\hat{\mathbf{e}}_{V}, \quad (6)$$

where $\epsilon$ is the fraction of the $\psi_{+}(\mathbf{r})\hat{\mathbf{e}}_{H}$ mode in the output power. Now, suppose that QWP-2 oriented at 0° and that the two arms of the Michelson interferometer are slightly misaligned, so that the wave vectors difference between the two outputs is $\delta\mathbf{k} = \delta k\hat{\mathbf{x}}$, orthogonal to the propagation axis. Taking into account the passage through the three half wave plates, and the transformation performed in each arm of the Michelson interferometer, we arrive at the following expression for the interference pattern:

$$I(\mathbf{r}) = 2|\psi(\mathbf{r})|^2[1 + 2\sqrt{\epsilon(1-\epsilon)}\sin 2\phi \sin(\delta kx)], \quad (7)$$

where $\phi = \arg(x + iy)$ is the angular coordinate in the transverse plane of the laser beam, and $|\psi(\mathbf{r})|^2$ is the doughnut profile of the intensity distribution of a Laguerre-Gaussian beam. It is clear from Eq. (7) that the visibility of the interference pattern is $2\sqrt{\epsilon(1-\epsilon)}$, which is precisely the concurrence of $\mathbf{E}_{\epsilon}(\mathbf{r})$ as given by Eq. (3). Therefore, the fringes visibility is related to the separability of the mode sent through the setup. However, the numerical coincidence with the concurrence is restricted to modes of the form given by Eq. (6). In fact, it is important to stress that the fringes visibility cannot be regarded as a measure of the concurrence for *any* nonseparable mode, but for our purposes it evidences the topological nature of the phase shift implemented by the experimental setup. A detailed discussion on the measurement of the concurrence is available in Ref. [15].

We now briefly discuss the quantum domain. When a partially nonseparable mode like $\mathbf{E}_{\epsilon}(\mathbf{r})$ is occupied by a single photon, this leads to a partially nonseparable single particle quantum state of the kind

$$|\varphi_{\epsilon}\rangle = \sqrt{\epsilon}|+H\rangle + \sqrt{1-\epsilon}|-V\rangle. \quad (8)$$

Experimentally, we attenuated the laser beam down to the single photon regime, and scanned a photocounting module across the interference pattern. First, HWP-A and B were set at 22.5° ($\epsilon = 1/2$) in order to evidence the topological phase in this regime. The $\pi$ phase shift could be clearly observed in this regime as well. The relationship between the fringes visibility and the state separability was evidenced by fixing QWP-2 at 0° and rotating HWP-A and B by an angle $\theta$ so that $\epsilon = \cos^2 2\theta$. Figure 4 shows the experimental results for the fringes visibility for several values of $\epsilon$. The solid line corresponds to the analytical expression of the concurrence, showing a very good agreement with the experimental values.

As a conclusion, we demonstrated the double connected nature of the $SO(3)$ rotation group and the topological phase acquired by a laser beam passing through a cycle of spin-orbit transformations. Such an effect was also observed using spins manipulated by magnetic fields [16]. We investigated both the classical and the quantum regimes and compared the separability of the mode traveling through the apparatus with the visibility of the interference fringes. Our results may constitute a useful tool for quantum computing and quantum information protocols.

The authors are deeply grateful to S. P. Walborn, P. H. Souto Ribeiro, and P. A. M. dos Santos. Funding was provided by Coordenação de Aperfeiçoamento de Pessoal de Nível Superior (CAPES), Fundação de Amparo à Pesquisa do Estado do Rio de Janeiro (FAPERJ-BR), and Conselho Nacional de Desenvolvimento Científico e Tecnológico (CNPq).

[1] S. Pancharatnam, Proc. Indian Acad. Sci. **44**, 247 (1956).
[2] M. V. Berry, Proc. R. Soc. A **392**, 45 (1984).
[3] J. A. Jones *et al.*, Nature (London) **403**, 869 (2000).
[4] L.-M. Duan, J. I. Cirac, and P. Zoller, Science **292**, 1695 (2001).
[5] S. J. van Enk, Opt. Commun. **102**, 59 (1993).
[6] E. J. Galvez *et al.*, Phys. Rev. Lett. **90**, 203901 (2003).
[7] M. J. Padgett and J. Courtial, Opt. Lett. **24**, 430 (1999).
[8] S. A. Werner *et al.*, Phys. Rev. Lett. **35**, 1053 (1975).
[9] P. Milman and R. Mosseri, Phys. Rev. Lett. **90**, 230403 (2003).
[10] P. Milman, Phys. Rev. A **73**, 062118 (2006).
[11] R. Mosseri and R. Dandoloff, J. Phys. A **34**, 10243 (2001).
[12] A. Yariv, *Quantum Electronics* (John Wiley & Sons, New York, 1988), 3rd ed.
[13] W. LiMing, Z. L. Tang, and C. J. Liao, Phys. Rev. A **69**, 064301 (2004).
[14] N. R. Heckenberg *et al.*, Opt. Lett. **17**, 221 (1992); G. F. Brand, Am. J. Phys. **67**, 55 (1999).
[15] S. Walborn *et al.*, Nature (London) **440**, 1022 (2006).
[16] J. Du *et al.*, arXiv:quant-ph/0705.3566.